DeepWind, 19–20 January 2012, Trondheim, NORWAY

Modelling the effect of ocean waves on the atmospheric and ocean boundary layers

Alastair D. Jenkins[a,*], Mostafa Bakhoday Paskyabi[b], Ilker Fer[b], Alok Gupta[c], Muralidhar Adakudlu[a]

[a]*Uni Computing & Bjerknes Centre for Climate Research, Geophysical Institute, Allégaten 70, N-5007 Bergen, Norway*
[b]*Geophysical Institute, University of Bergen, Allégaten 70, N-5007 Bergen, Norway*
[c]*Uni Computing, Høyteknologisenteret, Thormøhlensgate 55, N-5008 Bergen, Norway*

Abstract

Ocean waves, in addition to generating direct forces on fixed and floating offshore wind generator structures, also have significant indirect effects via their influence on the atmospheric and oceanic boundary layers above and below the water surface. In the atmospheric boundary layer the waves act as roughness elements, influencing the turbulent flow and the vertical wind speed profile, and induce oscillatory motions in the airflow. Spray droplets from breaking wave crests enhance structure corrosion, and may lead to icing under low-temperature conditions. Below the water surface, the air-sea momentum flux and mechanical energy flux, mediated by the waves and wave-generated turbulence, affect the vertical profiles of ocean current, temperature, and salinity. Effects include modifying the structural forces and dynamics, and the movement and dispersion of marine organisms, pollutants, and air bubbles generated by breaking waves, with consequences for fouling, corrosion, and environmental impact. Measurement of relevant airflow and ocean dynamical variables is also challenging, as near the water surface it is often necessary to use instruments mounted on moving measurement platforms.

Modelling such boundary-layer effects is a complex task, as a result of feedbacks between the airflow, wave field, current field, and turbulence in the atmosphere and the ocean. We present results from a coupled model study of the North Sea and Norwegian Sea area. We employ a mesoscale atmosphere model (WRF) and a spectral wave model (WAM), running simultaneously and coupled using the open-source coupler MCEL which can interpolate between different model grids and time steps. To investigate the ocean boundary layer, one-dimensional model experiments were performed for an idealized Ekman layer and for locations in the North Sea, Atlantic Ocean, and the northern Pacific, using a version of the GOTM turbulence model, modified to take wave dynamics into account.

Results show how the wave field alters the ocean's aerodynamic roughness and the air–sea momentum flux, depending on the relation between the surface wind speed and the propagation speed of the wave crests (the wave age). These effects will feed back into the airflow, wind speed and turbulence profile in the boundary layer. The ocean dynamics experiments showed results which compare favourably with field observations from the LOTUS3 and PROVESS experiments in the north Atlantic and North Sea, and Ocean Weather Station Papa in the Pacific Ocean.

© 2012 Published by Elsevier Ltd. Selection and/or peer-review under responsibility of SINTEF Energi AS.

Keywords: ocean waves, atmospheric boundary layer, ocean surface boundary layer, numerical modelling

*Corresponding author
Email address:* alastair.jenkins@uni.no (Alastair D. Jenkins)

1. Introduction

Since ocean waves have considerable energy, they obviously effect substantially the design, operation, and maintenance of offshore wind power production facilities. These effects may be direct, or they may result from their influence on the adjacent atmospheric and oceanic boundary layers.

Direct effects. The hydrostatic pressure changes and orbital velocities and fluid accelerations induced in the water column by surface waves produce direct forces on wind generator structures. Breaking waves, by direct impact of the steeply-sloping crest, induce impulsive, 'slamming' forces. Salt spray generated by the breakup of water jets from breaking crests, enhances corrosion, and leads to increased superstructure icing at low air temperatures. Air bubbles generated by the impact of the breaking crest surface, breaker jet, and spray droplets with the water surface, and carried down into the water column with the turbulent motions, may also enhance corrosion and will affect marine fouling and other biological processes.

Indirect effects: Effect on the atmosphere. Waves influence the airflow by processes related to that described by Miles [1]. Waves induce oscillations in the airflow, which interact with the mean airflow in the turbulent atmospheric boundary layer, primarily near the critical height z_c where the wind speed $U(z_c)$ is equal to the wave phase velocity c. This interaction induces pressure fluctuations on the water surface in phase with the surface slope, causing transfer of energy and momentum from the mean airflow to the wave field. The effect of the momentum transfer on the airflow was calculated by Janssen [2] and Jenkins [3], among others. The dependence of the air–sea momentum flux on the wave field may be approximated by a wave-dependent aerodynamic roughness length z_0, or, alternatively, by a varying coefficient α in the Charnock [4] relation

$$z_0 = \alpha u_*^2/g \qquad (1)$$

where $u_* = \sqrt{\tau/\rho_a}$, τ being the wind stress (air–sea momentum flux) and ρ_a the air density. Changes in z_0 feed back into the vertical profile $U(z)$ of wind speed (under neutral conditions) via the logarithmic turbulent boundary-layer relation:

$$U(z) = (u_*/\kappa) \log(z/z_0), \qquad (2)$$

where $\kappa \approx 0.4$ is the von Kármán constant.

Effect on the ocean. Wave effects on the ocean are primarily the result of wave-induced drift (the Stokes drift due to the non-closure of wave-induced orbital paths, when integrated vertically, is equal to the momentum of the wave field divided by the water density). Depending upon whether an Eulerian or a Lagrangian mean formulation is used for the mean current, a 'Coriolis–Stokes' term, due to the Coriolis acceleration acting on the Stokes drift, appears in the equations of motion. The Stokes production of TKE as a responsible factor between the Reynolds stresses and surface gravity waves appears as a source term in the turbulent kinetic energy and dissipation rate equations.

Wave orbital motions can also induce turbulence and mean flows near the sea bottom, which have important effects on sediment transport and foundation scouring. These processes will, however, be addressed in a later study.

Numerical modelling approaches. In this paper we show results of numerical model simulations using publically available source code: for the atmosphere, we apply the Weather Research and Forecasting (WRF) model [5] (`http://wrf-model.org`), coupled to the WAM third-generation spectral wave model [6]. Various different coupling algorithms have been applied to calculate the effect of ocean waves on the atmospheric boundary layer, e.g., [7, 8]. For computational economy, we apply the scheme of Janssen [9], applied to coastal and shelf seas by Brown and Wolf [10].

To calculate the effect of waves on the the ocean surface boundary layer we apply a modified version of the one-dimensional General Ocean Turbulence Model (GOTM) [11] (`http://www.gotm.net`).

2. Coupled atmosphere—ocean wave model study

2.1. Model system

Atmosphere model. The Weather Research and Forecasting (WRF) model [5] is a state-of-the-art non-hydrostatic mesoscale numerical model of the atmosphere, developed for numerical weather prediction and related applications. For the present study, we employed a domain with $30\,\mathrm{km} \times 30\,\mathrm{km}$ grid spacing in a polar stereographic projection, and applied the default YSU planetary boundary-layer scheme and with default Monin–Obukhov surface-layer physics, modified to import a variable Charnock coefficient (see Eq. 1) calculated from the wave model variables every 60 minutes, using the MCEL coupling scheme (see below).

Wave model. To compute the ocean wave field we employ the third-generation spectral wave model WAM [6], Cycle 4, over the geographical domain shown in Fig. 1 with a grid spacing of $0.2°$ longitude $\times\,0.2°$ latitude. The model is driven by the wind speed and direction at a height of 10 metres, supplied every 60 minutes and interpolated to the WAM model grid by the MCEL coupling scheme.

The WAM model computes the air-to-sea momentum flux τ_w associated wave generation, from the computed wave energy input source terms, and also the total air-to-sea momentum flux $\tau = \rho_a u_*^2$. The quantities τ_w/τ and u_* are fed back to the WRF atmosphere model every 60 minutes by the MCEL coupling scheme. We apply the coupling algorithm of Janssen [9], applied to coastal and shelf seas by Brown and Wolf [10].

Model coupling. We apply the Model Coupling Environment Library (MCEL) [12][1], a CORBA-based client-server based coupling framework, which may be used for coupling numerical models with differing domains and grid resolutions. In the present study the WAM wave model domain covers part of the WRF atmosphere model domain, and the grid map projections are also different (latitude/longitude and polar stereographic, respectively). The MCEL scheme interpolates variables between the different grids, every 60 minutes in the present instance.

Within the WRF model surface-layer routine, we apply the algorithm of Janssen [9] and Brown and Wolf [10] as follows: If wave-model information is available, the surface roughness length is computed from the quantities τ_w/τ and u_* supplied from the WAM model:

$$\alpha_v = \min\left(\frac{\alpha_{\min}}{\sqrt{1 - (\tau_w/\tau)}}, \alpha_{\max}\right), \tag{3}$$

$$z_0 = (\alpha_v u_*^2/g) + z_{0\min}, \tag{4}$$

where α_v is the variable Charnock parameter, $\alpha_{\min} = 0.01$ and $\alpha_{\max} = 0.31$ are its minimum and maximum values, respectively, and $z_{0\min} = 1.59 \times 10^{-5}$ m is the minimum roughness length. Where no wave-model information is available, a constant Charnock parameter of 0.0185 is used instead of α_v in (4).

2.2. Results

Figure 1 shows selected WAM wave model results after 24 hours' model simulation, including significant wave height, wave direction, and peak wave frequency. The main result is that the Charnock parameter and roughness length are enhanced where the waves are developing rapidly and the sea is not fully developed. This occurs where the wind is changing rapidly with time or where the fetch is reduced (the wind is blowing offshore), both situations may be described as 'young wave' conditions with a low *wave age* c_p/u_*, where c_p is the celerity of the dominant waves.

An example of the effect on the WRF model results is shown in Fig. 2, which shows the development of the roughness length over the 48-hour simulation. Where wave information is available, the roughness length does tend to be increased, particularly where the wind changes rapidly or the fetch is short. This effect will tend to produce a reduced wind speed and increased amount of turbulence at a $O(100\,\mathrm{m})$ wind turbine height.

---

[1]See also J. Michalakes, 2003, Infrastructure Development for Regional Coupled Modeling Environments, `http://www.mmm.ucar.edu/wrf/WG2/Tigers/IOAPI/index.html` .
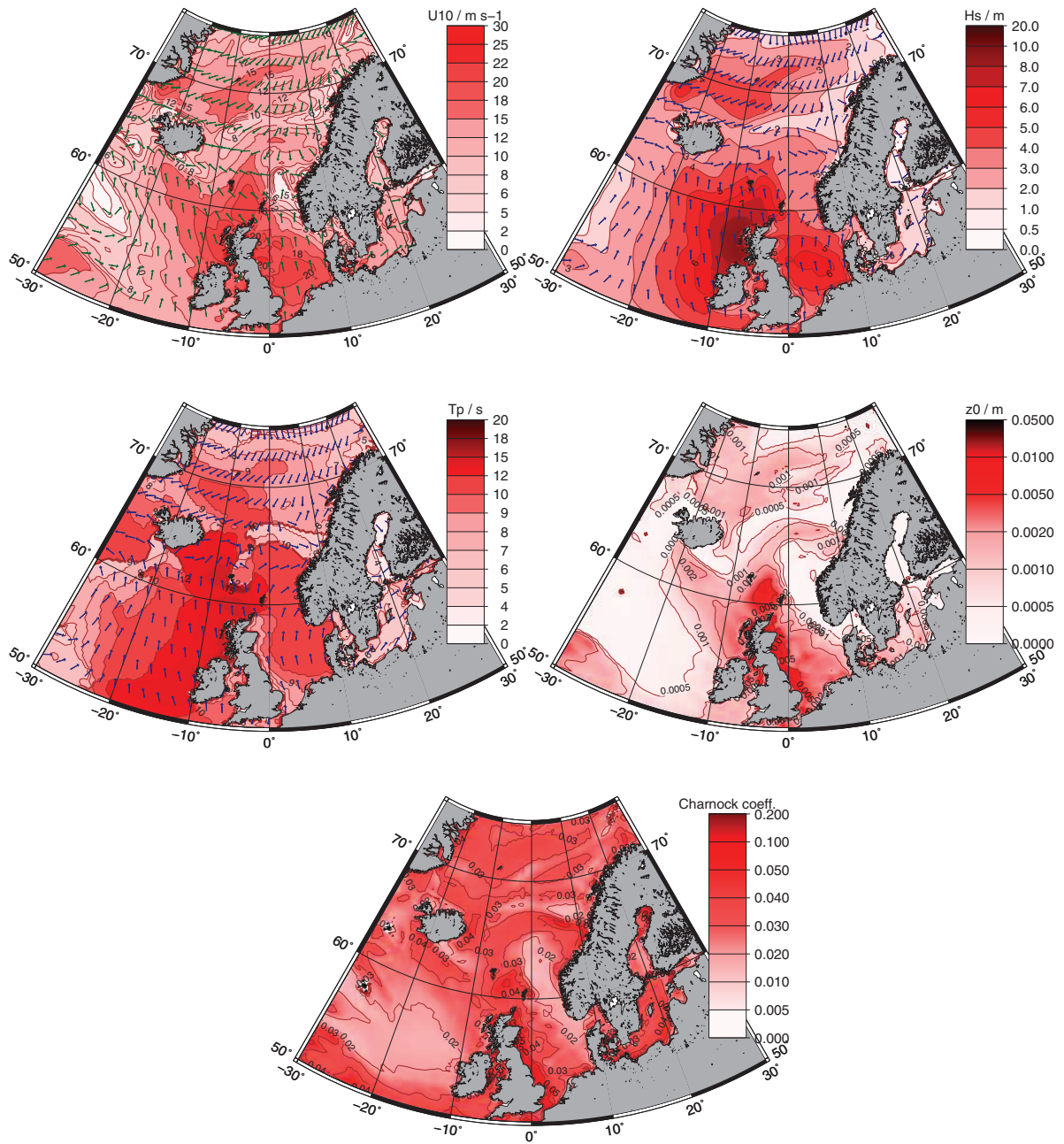
Fig. 1. WAM wave model results after 24 hours' simulation from the coupled WRF–WAM atmosphere–wave model run. *Top left*: Wind speed at 10 m height and wind direction interpolated from the WRF model. *Top right*: Significant wave height and peak wave direction. *Centre left*: Peak wave period and direction. *Centre right*: Roughness length computed from the wave-induced air–sea stress. *Bottom*: Charnock parameter computed from the wave-induced and total air–sea stress.
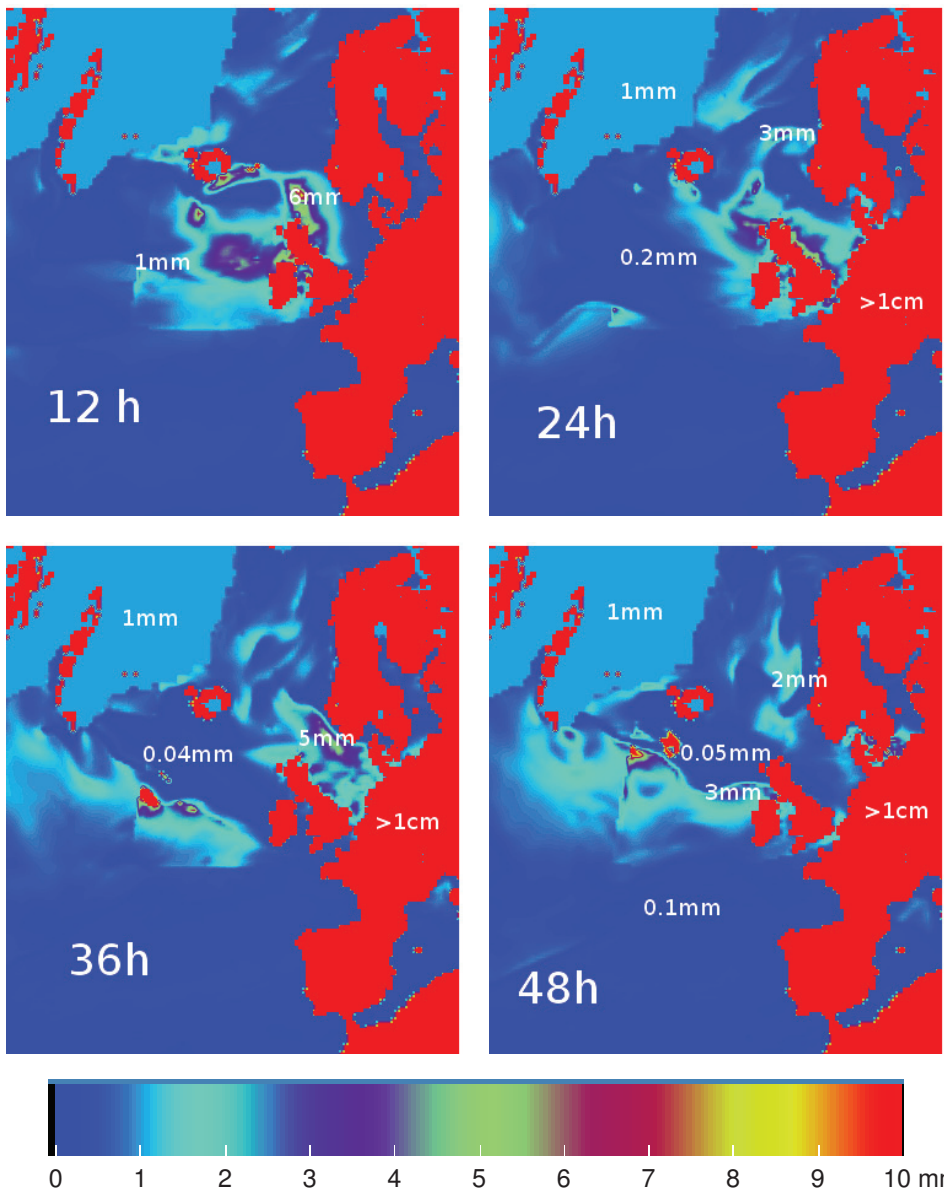
Fig. 2. Roughness length over the ocean computed by the WRF model during the WRF–WAM atmosphere–wave model simulation, from the variable Charnock parameter computed using the wave-model-calculated wave-induced and total air–sea stress. The roughness length over the Greenland ice sheet and land areas is indicated for comparison. A discontinuity can generally be seen in the roughness length at the boundary of the wave model domain (the parallel 50°N and the meridian 30°W).

A preliminary comparison of with corresponding WRF and WAM model results for one-way coupling (WRF to WAM only) shows a slight reduction in wind speed and wave height for the two-way coupling case.

3. Ocean boundary layer study

The interaction of the turbulent Reynolds stress with the shear of wave generated Stokes drift can enhance upper ocean mixing for both breaking and non-breaking waves. In this study, we modify the turbulent

kinetic energy (TKE) and the dissipation rate of TKE in the governing equations of the General Ocean Tur-
bulence Model (GOTM) [11] by including the Stokes production of the TKE term. It should be noted that
in this paper, the role of non-breaking waves in transferring energy to the upper ocean mixing (the so-called
wave–turbulence interaction) is studied by including the Stokes production of TKE in the energy equations.
This is different from the modifications presented in [13] in which the dominant role of Stokes drift has
been applied by adding the Coriolis–Stokes force to the momentum equations.

3.1. Ocean modelling techniques

According to [14, 15], the wave–turbulence modified energy equations can be described based on a k-ϵ
closure model

$$\frac{\partial k}{\partial t} = P_s + P_w + P_b - \epsilon + \mathcal{D}(k) \tag{5}$$

$$\frac{\partial \epsilon}{\partial t} = \frac{\epsilon}{k}(C_1(P_s + P_w) + C_3 P_b - C_2 \epsilon) + \mathcal{D}(\epsilon), \tag{6}$$

where P_s, P_w, and P_b are shear production, the Stokes production of TKE, and the buoyancy produc-
tion/dissipation, respectively. The coefficients C_1, C_2, and C_3 are calibration constants, and $\mathcal{D}(.)$ is the sum
of the turbulent and viscous transport terms [16]. The Stokes production of TKE is computed as

$$P_w = -\rho_w \overline{u'w'}\frac{\partial U_s(z)}{\partial z} - \rho_w \overline{v'w'}\frac{\partial V_s(z)}{\partial z} \tag{7}$$

where $-\rho_w \overline{u'w'}$ and $-\rho_w \overline{v'w'}$ are the components of the Reynolds stress. $U_s(z)$ and $V_s(z)$ are the components
of the wave–generated Stokes drift. In this study, P_w is calculated by a simple formula given in [15].

The modified boundary condition at the sea surface is

$$\nu_t \frac{\partial \mathbf{U}}{\partial z} = \frac{1}{\rho_o}\left(\vec{\tau}_{tot} - \vec{\tau}_{in}\right), \tag{8}$$

where ν_t is the turbulent eddy viscosity, $\mathbf{U}$ is the current, ρ_o is the water density, and $\vec{\tau}_{tot}$ and $\vec{\tau}_{in}$ are the total
wind stress and wave-induced momentum, respectively. Following [17], the surface energy flux boundary
condition induced by the wave breaking is formulated as $\alpha\rho_a u_*^2$ with constant $\alpha = 100$. For the lower
boundary condition at the sea bottom, a zero flux of turbulent energy is assumed.

3.2. Comparison with measurements

Two test cases have been constructed to study various features of the wave effects on the oceanic bound-
ary layer on diurnal and seasonal time scales. The wave field has been modelled by the Donelan–Pierson
(DP) wave spectrum. The Mixed Layer Depth (MLD) is inferred from the potential density profile following
[13]. In both scenarios, the wave–turbulence interaction (WTI) modified GOTM results are compared with
observations and results reported by [13] (hereafter, Ba12).

PROVESS. Here, we apply the modified GOTM model to the data set from PROVESS experiment in the
northern North Sea. The site is located at 59.3°N and 1°E and the water depth is 110 m. A 20-day period
between 7 and 27 October 1966 is chosen and analysis of the whole water column for this period is confined
only to dynamics of the surface mixed layer. The atmospheric forcing, wind stress and heat flux strongly
increase after the first seven days. Fig. 3 (top)-a,b,c shows a comparison of the temporal structure of tem-
perature among (a) observations, (b) WTI-modified GOTM simulation, and (c) simulation results without
the modification. Fig. 3 (bottom) shows that the WTI modification gives a better estimate of the temporal
variability of the heat content of the upper 50 metres compared to the results of Ba12 for the same scenario
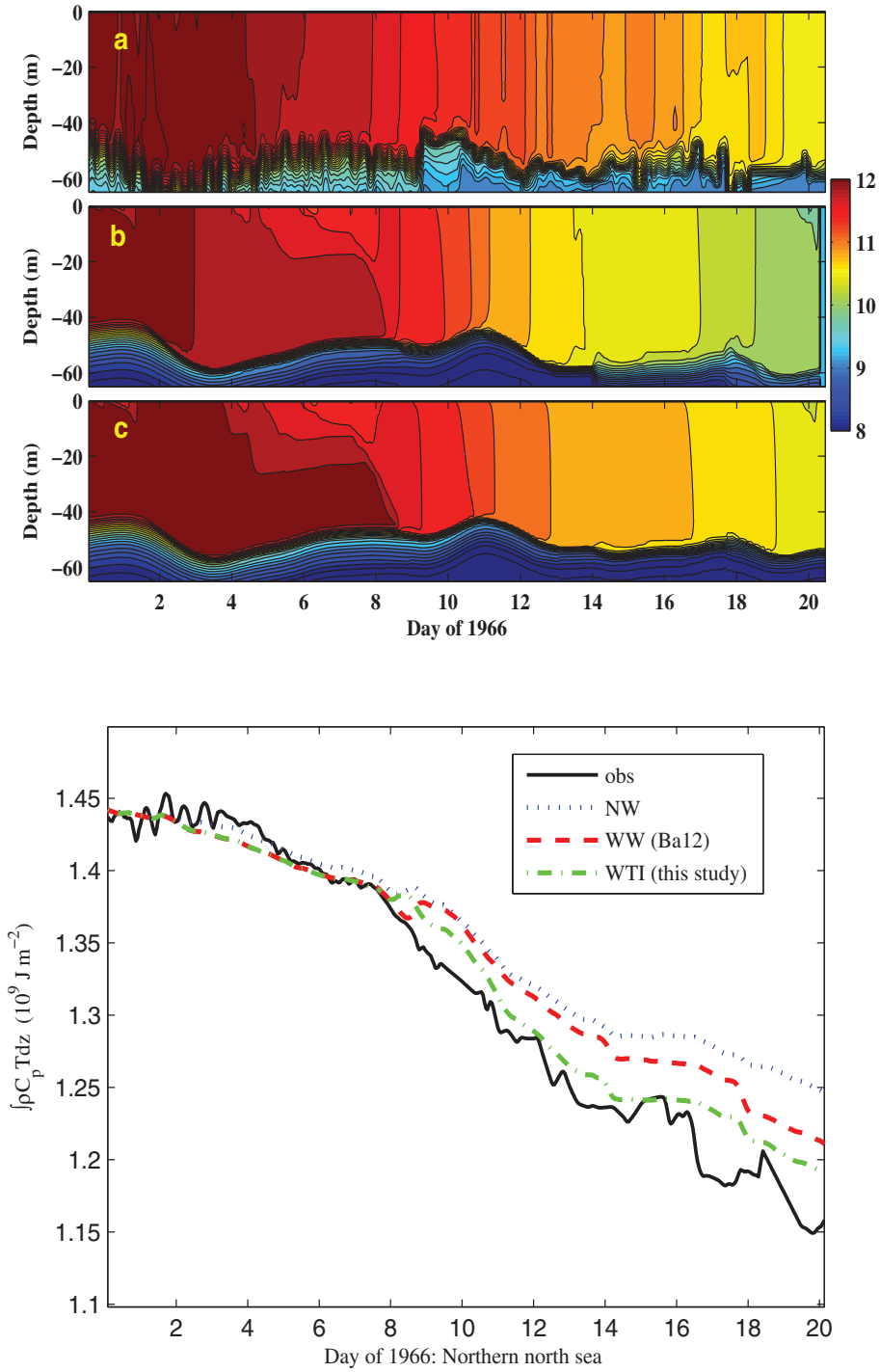and no wave forcing.

Fig. 3. *Top*: Depth–time evolution of the upper layer temperature for a period between 7 and 27 October 1966 in the northern North Sea for (a) observed temperature, (b) the WTI-modified GOTM modelled temperature, and (c) the simulation without wave forcing. *Bottom*: (a) Temporal variability of the heat content in the upper 50 m.

OWS Papa. Ocean Weather Station (OWS) Papa long term observations of meteorological parameters and temperature profiles (at 50°N, 145°W) are applied as a final validation test case for the whole of year 1966. Figure 4 (top) shows the results of the simulated temperature for (a) observations, (b) simulation results based on Ba12, (c) WTI-modified GOTM results, and (d) no wave forcing. Similar to the PROVESS test case, the heat content of the upper 50 m, MLD evolution, and temperature evolution at OWS Papa show that the WTI-based modification captures the observations better than the Ba12-modified GOTM results.

3.2.1. Discussion

The observations have shown that swell-induced motion can transport turbulence downward [18]. This wave–turbulence interaction enhances mixing and conducts the surface heat into interior water column beneath. In this study, the Stokes production of TKE as a responsible factor of the WTI effect is included in GOTM by modifying the TKE and TKE dissipation rate equations. To evaluate the skill of the WTI-modified GOTM, a series of model experiments are conducted to cover some features of upper ocean boundary layer on diurnal and seasonal time scales. The modelled results show that including WTI reproduces the observed temperature evolution and MLD dynamics. Furthermore, WTI simulation gives a more realistic behaviour and transfers more heat from the surface to the subsurface water column than that reported in Ba12. However, there are some sources of errors in the model results that can be attributed to absence of advection, uncertainty in net surface heat flux calculation, idealized sea state assumption, measurement errors in hydrography and current meters attached to surface floats, bottom friction effects, and sea surface roughness parameterization.

4. Conclusion

In this investigation we have applied a number of numerical modelling techniques to investigate the effect of ocean waves on the atmospheric and upper ocean boundary layers in ways that may impact wind power production. The models applied were the WRF mesoscale atmosphere model, coupled in both directions with the WAM Cycle 4 spectral wave model, to compute the wave–atmosphere interaction. Wave–ocean interaction was computed using a WTI-modified version of the GOTM ocean turbulence model.

The wave–atmosphere interaction results consisted primarily of an enhancement of the surface aerodynamic roughness during rapidly-developing and short-fetch conditions. The coupling method used was to exchange data every 60 minutes to alter the Charnock parameter relating the friction velocity and roughness length, computed from the momentum flux extracted from the atmosphere by growing waves. The results indicate a modest reduction of mean wind speed and increase in turbulence intensity at wind turbine hub height. Since the wave-induced momentum flux may differ in direction from that of the wind itself, it may be advantageous to allow for a difference in the directions of wind and wave-induced stress and wind velocity in subsequent versions of the coupled model system.

The wave–ocean interaction experiments show that including the wave forcing captures better the observed temperature evolution and mixed-layer dynamics compared to the no-wave case and the Ba12-modified GOTM results. The Stokes drift is a dominant wave effect. Its vertical gradient interacts with the turbulent Reynolds stress resulting in enhanced mixing and increased heat transport from the surface to the water column. There are some uncertainties in the results as a consequence of advection contaminating the one-dimensional model scheme, and future studies should ideally incorporate more detailed measurements in the near-surface layer of the ocean and a better estimate of breaking-wave effects. Since waves themselves have a significant effect on forces on wind turbine foundations, cabling, sediment transport, and the marine environment, such additional measurements are certainly justified.
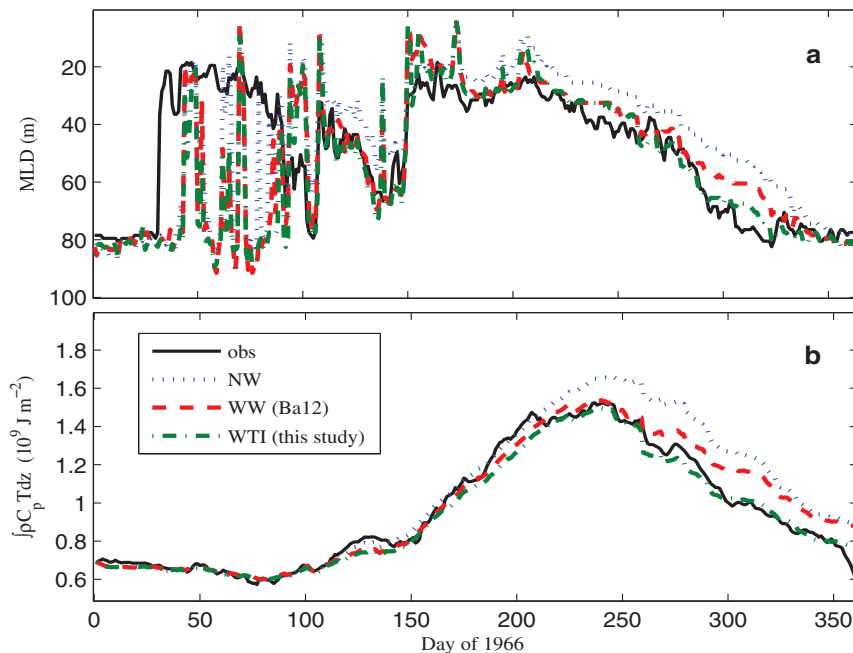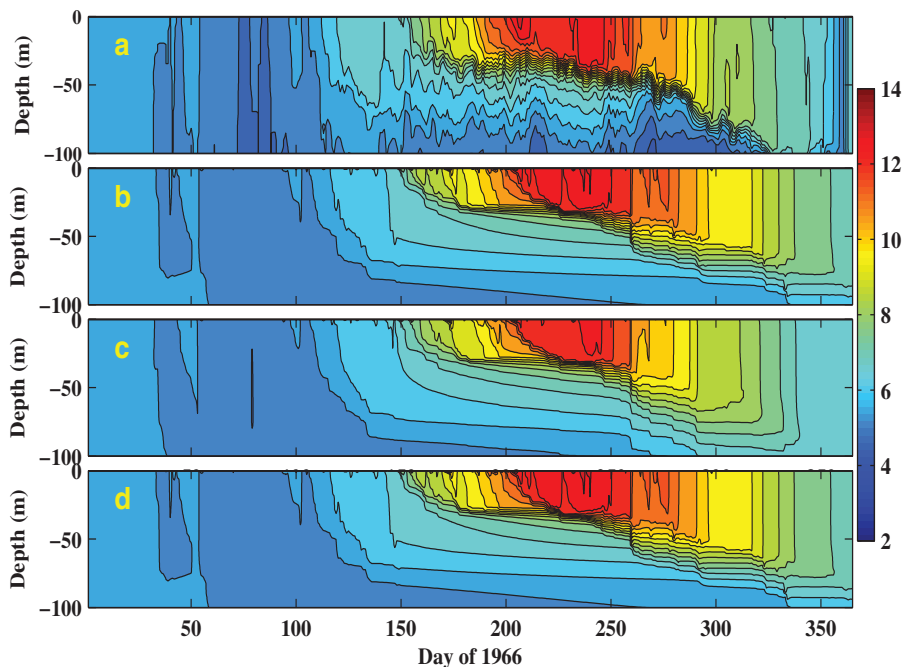
Fig. 4. *Top*: Temperature evolution at OWS Papa in the northern Pacific Ocean for year 1966, (a) observations, (b) GOTM run with wave forcing effects based on [13], (c) GOTM with the wave–turbulence interaction modification, (d) GOTM without wave forcing. *Bottom*: Temporal variability of (a) MLD and (b) heat content in the upper 50 m.

References

[1] J. W. Miles, On the generation of surface waves by shear flows, Journal of Fluid Mechanics 3 (1957) 185–204.

[2] P. A. E. M. Janssen, Wave-induced stress and the drag of air flow over sea waves, Journal of Physical Oceanography 19 (1989) 745–754.

[3] A. D. Jenkins, A quasi-linear eddy-viscosity model for the flux of energy and momentum to wind waves, using conservation-law equations in a curvilinear coordinate system, Journal of Physical Oceanography 22 (8) (1992) 843–858.

[4] H. Charnock, Wind stress on a water surface, Quarterly Journal of the Royal Meteorological Society 81 (1955) 639–640.

[5] W. C. Skamarock, J. B. Kemp, J. Dudhia, D. O. Gill, D. M. Barker, W. Wang, J. G. Powers, A description of the Advanced Research WRF Version 2 (2005).

[6] The WAMDI Group, The WAM model—a third generation ocean wave prediction model, Journal of Physical Oceanography 18 (12) (1988) 1775–1810.

[7] A. Rutgersson, Ø. Sætra, A. Semedo, B. Carlsson, R. Kumar, Impact of surface waves in a regional climate model, Meteorologische Zeitschrift 19 (2010) 247–257.

[8] B. Liu, H. Liu, L. Xie, C. Guan, D. Zhao, A coupled atmosphere–wave–ocean modeling system: Simulation of the intensity of an idealized tropical cyclone, Monthly Weather Review 139 (2011) 132–152.

[9] P. A. E. M. Janssen, Quasi-linear theory of wind-wave generation applied to wave forecasting, Journal of Physical Oceanography 21 (1991) 1631–1642.

[10] J. M. Brown, J. Wolf, Coupled wave and surge modelling for the eastern Irish Sea and implications for model wind-stress, Continental Shelf Research 29 (2009) 1329–1342, postprint available from institutional archive: `http://nora.nerc.ac.uk/8088/1/post_print.pdf`. doi:10.1016/j.csr.2009.03.004.

[11] H. Burchard, Applied Turbulence Modelling in Marine Waters, Springer, Berlin, 2002, vol. 100 of Lecture Notes in Earth Sciences.

[12] M. T. Bettencourt, Distributed model coupling framework, in Proc. HPDC-11, July 2002 (2002).

[13] M. Bakhoday-Paskyabi, I. Fer, A. D. Jenkins, Surface gravity wave effects on the upper ocean boundary layer: modification of a one-dimensional vertical mixing model, Continental Shelf Research (accepted) (2011).

[14] L. H. Kantha, C. A. Clayson, On the effect of surface gravity waves on mixing in the oceanic mixed layer, Ocean Modelling 6 (2004) 101 – 124.

[15] C. J. Huang, F. Qiao, Z. Song, T. Ezer, Improving simulation of the upper ocean by inclusion of surface waves in the Mellor-Yamada turbulence scheme, Journal of Geophysical Research 116 (2011) C01007, doi:10.1029/2010JC006320.

[16] H. Burchard, K. Bolding, Comparative analysis of four second-moment turbulence closure models for the oceanic mixed layer, Journal of Physical Oceanography 31 (2001) 1943–1968.

[17] P. D. Craig, M. L. Banner, Modeling wave-enhanced turbulence in the ocean surface layer, Journal of Physical Oceanography 24 (1994) 2546–2559.

[18] A. Anis, J. N. Moum, Surface wave—turbulence interactions: Scaling $\epsilon(z)$ near the sea surface, Journal of Physical Oceanography 25 (1995) 2025–2045.